F−V/SMS: A New Technique for Studying the Structure and Dynamics of Single Molecules and Nanoparticles†

Andre J. Gesquiere, So-Jung Park, and Paul F. Barbara*

Center for Nano- and Molecular Science and Technology, Department of Chemistry and Biochemistry, University of Texas at Austin, Austin, Texas 78712

Received: January 29, 2004

We recently introduced a new technique for semiconductor nanoparticle research that involves simultaneous single molecule spectroscopy (SMS) *and* controllable oxidation/reduction in an electronic device. This paper shows that the new technique, denoted by fluorescence-voltage single molecule spectroscopy (F−V/SMS), is analogous to current vs voltage (*I*−*V*) measurements for devices and electrochemical cells. F−V/SMS data are reported for single molecules (nanoparticles) of the conjugated polymer MEH−PPV as a function of bias voltage on the device and bias sweep rate to obtain information on both the energetics and kinetics of the charge transfer (oxidation/reduction) process in situ on the nanoscale. The extensive F−V/SMS data presented herein reveal that the dynamics for oxidation/reduction of MEH−PPV nanoparticles are controlled by various factors including filling of deep hole traps in the charge transporting layer of the device, the oxidation/reduction chemical "state" of the MEH−PPV molecule, and the molecular scale heterogeneity of the device.

Introduction

Single molecule spectroscopy (SMS) has proven to be a unique and powerful tool for the investigation of functional semiconductor nanomaterials, including semiconductor nanocrystals,[1−9] and nanostructured conjugated polymers.[10−21] The complex photophysical processes of these heterogeneous materials are often obscured in ensemble measurements, but become accessible by single molecule (single particle) methods. For example, SMS has been used extensively to study the molecular structure and photophysical dynamics of single *isolated* polymer chains (molecules) of conjugated polymers.[10−12,14,22] On the nanoscale, conjugated polymers have complex nanostructure associated with polymer chain folding, packing, and aggregation. The spectroscopy of single polymer chains, as opposed to the bulk material, has the advantage of tremendously reducing the "size" and complexity of the sample under investigation in a single experiment. SMS has led to the following discoveries for conjugated polymers:

(i) conjugated polymers have surprisingly ordered conformations;

(ii) singlet excitons are efficiently "funneled" to a small number of sites (even a single site) in a large (MW $\sim 10^6$) single polymer chain; and

(iii) photooxidation occurs in conjugated polymer nanoparticles through the generation of single quenching sites, which act as extremely efficient fluorescence quenchers.[11,12]

Semiconductor nanoparticle materials have a number of important device applications, such as light-emitting displays, solar cells, chemical sensors, and related devices.[23−27] Unfortunately, nanomaterial-based devices are highly complex, involving a large number of interactions among a diverse set of electronically excited states (excitons), charge carriers (polarons), and chemical intermediates of various forms and energies. The complexity and heterogeneity of nanomaterial-based devices is a major obstacle to the effective investigation of these devices by bulk ensemble measurements, such as current−voltage (*I*−*V*) measurements and photoluminescence studies.[28−32]

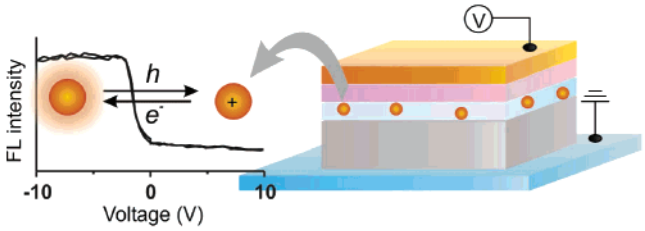

Figure 1. Sketch of the device structure used in the F−V/SMS studies. MEH−PPV nanoparticles (orange dots), sitting on top of an insulating layer (grey), are close to or contacting a hole transporting layer (HTL, red), which is in turn interfaced with a gold electrode (yellow) at which hole injection occurs. F−V/SMS data for a single electron-transfer involving a single MEH−PPV nanoparticle are shown on the left.

We recently introduced a new technique that allows for SMS of nanoparticles in a device environment. The method involves simultaneous single molecule fluorescence spectroscopy *and* controllable oxidation/reduction on an individual nanoparticle in an electronic device (Figure 1).[33] The technique is ideally suited for studying the interaction of excitons and polarons. This is achieved by recording the SMS fluorescence intensity as a function of device bias, which in turn controls the population of polarons in the nanoparticle. The new approach also offers a unique handle on the chemical nature of the poorly understood photochemically prepared intermediate states of a nanoparticle that are responsible for fluorescence "blinking" and "flickering", i.e., intermittency. By studying the bias dependence of the SMS during the lifetime of the fluorescence "flickering" intermediate, information on the oxidation/reduction properties (e.g., HOMO energies) of the intermediate can be determined. In particular, we have applied the technique to elucidate the chemical structure

† Part of the special issue "Gerald Small Festschrift".

* Author to whom correspondence should be addressed. E-mail: p.barbara@mail.utexas.edu.

10.1021/jp049583f CCC: $27.50
Published on Web 04/21/2004

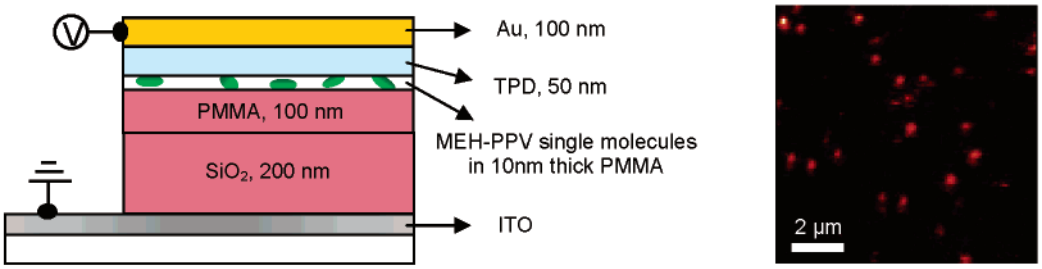

Figure 2. *Left*: Detailed representation of the structure of the single-molecule capacitor device. *Right*: Single molecule spectroscopy confocal sample scanning image of the device. Well-isolated, bright fluorescence spots with an average separation of ~1−2 μm can be observed. Each bright spot in the image corresponds to the location of a single conjugated polymer nanoparticle.

of photooxidized intermediates in the photobleaching of poly[2-methoxy, 5-(2′-ethylhexyloxy)-*p*-phenylenevinylene] (MEH−PPV) in an electronic device structure.[33]

This paper is focused on the further development of the SMS/charge injection technique for semiconductor nanoparticle research. The SMS fluorescence intensity is recorded for MEH−PPV single molecules (nanoparticles) as a function of bias voltage on the device, using a linear sweep rate. The technique, which we denote by F−V/SMS (where "F" signifies fluorescence intensity), is analogous in several ways to current vs voltage ($I-V$) measurements for devices and electrochemical cells. For example, it will be shown below that, in analogy to the $I-V$ technique, F−V/SMS data as a function of sweep rate can be analyzed to obtain information on both energetics and kinetics of the charge transfer (oxidation/reduction) process in situ on the nanoscale. The extensive F−V/SMS data presented herein reveal that the dynamics for oxidation/reduction of MEH−PPV nanoparticles are controlled by various factors including filling of deep hole traps[34,35] in the charge transporting layer of the device, the oxidation/reduction chemical "state" of the MEH−PPV molecule, and the molecular scale heterogeneity of the device.

Experimental Section

Device Fabrication. The combined single molecule spectroscopy−charge injection devices employed a large area (1 cm^2) multilayer structure, as shown in Figure 2. The structure was fabricated bottom-up on top of an indium tin oxide (ITO) coated quartz cover slip (Metavac) by e-beam evaporation (SiO_2), spin-coating (poly(methyl methacrylate)(PMMA) layer and MEH−PPV/PMMA layer), and finally thermal evaporation of a *N*,*N*′-bis(3-methylphenyl)-*N*,*N*′-diphenylbenzidene (TPD) charge transport layer and Au electrode. The upper PMMA/MEH−PPV layer was spin-coated from the relatively poor PMMA solvent toluene to minimize erosion of the lower PMMA layer, which was spin-coated from chloroform. The SiO_2 layer served to electrically insulate the ITO electrode. The lower PMMA layer further helped block charges from ITO due to conduction by pinholes in SiO_2, and also served to isolate MEH−PPV molecules from the SiO_2 surface, i.e., where MEH−PPV molecules exhibit photoinstability in experiments without the PMMA spacer layer. Layer thickness and rms roughness were measured by atomic force microscopy (AFM) for representative, partially fabricated devices. The PMMA and MEH−PPV/PMMA layers had a rms roughness of <1 nm per square micrometer. The TPD layer, however, revealed a rms roughness of >2 nm per square micrometer due to apparent nanocrystallization. This morphological structure of the TPD layer appeared to vary from device to device, which may account for the large device-to-device variations observed herein (see below).

Single Molecule Spectrocopy. Single molecule spectroscopy confocal sample scanning images (Figure 2) of the devices revealed well-isolated, bright fluorescence spots with an average separation of ~2 μm, which was set by controlling the spin-coating conditions and the concentration of MEH−PPV in MEH−PPV/PMMA solutions. Fluorescence vs time traces for single MEH−PPV molecules were obtained by moving the sample stage to a chosen molecule and recording the fluorescence vs time with a home-built multichannel scaler, continuously irradiating the molecule with ~2500 W cm^{-2} of 514.5 nm light focused at the diffraction limit by a 100×, 1.25 NA Carl Zeiss achrostigmat objective lens. Other SMS experimental details were similar to previous reports.[36]

F−V/SMS Experiments. For the F−V/SMS experiments, electrodes were attached to the ITO and Au electrodes of the devices by means of silver epoxy (Dynaloy Inc.). A repetitive waveform (usually triangular) was applied to the device during the recording of the SMS intensity vs time data with the multichannel scaler. The multichannel scaler data acquisition was synchronized to the voltage waveform to allow for synchronized averaging of the data vs time and bias over many cycles of the applied electrical bias.

Device Architecture and Materials

The MEH−PPV (Uniax Corp.) molecules in this study have an average molecular weight of ~500,000 amu with ~1700 monomer units in a typical polymer chain. Isolated MEH−PPV molecules in the PMMA matrix are predicted to be cylindrically shaped with a long axis of ~15 nm.[10] Isolated conjugated polymer single molecules behave as a coupled multi-chromophoric system due to interruptions of the conjugation by disorder along the polymer chain.[10,11] For the MEH−PPV molecules in this study, there are ~200 effective chromophores on the polymer chain, each with 10−17 repeat units in conjugation length.

The device architecture employed herein (Figure 2) is roughly analogous to an organic LED that has been modified by replacing the electron transport layer/luminescence layer with a charge blocking layer. In analogy to OLEDs, holes should be injected into TPD creating a hole space charge at biases comparable to and greater than the inner potential V_{ip} of the device, which can be estimated from the work function differences in the device.[37−41] Hole neutralization at the ITO electrode is suppressed by the PMMA and SiO_2 layers, and holes are predicted to pile up at the TPD/MEH−PPV/PMMA interface at positive bias voltages. In contrast, at high negative bias, holes should be removed from the TPD layer. The work function of Au is too large to allow for electron injection into TPD over the bias ranges relevant herein.[41] Qualitatively, as the bias of the device is increased from negative bias to positive bias, the density of holes at the TPD/MEH−PPV interface should

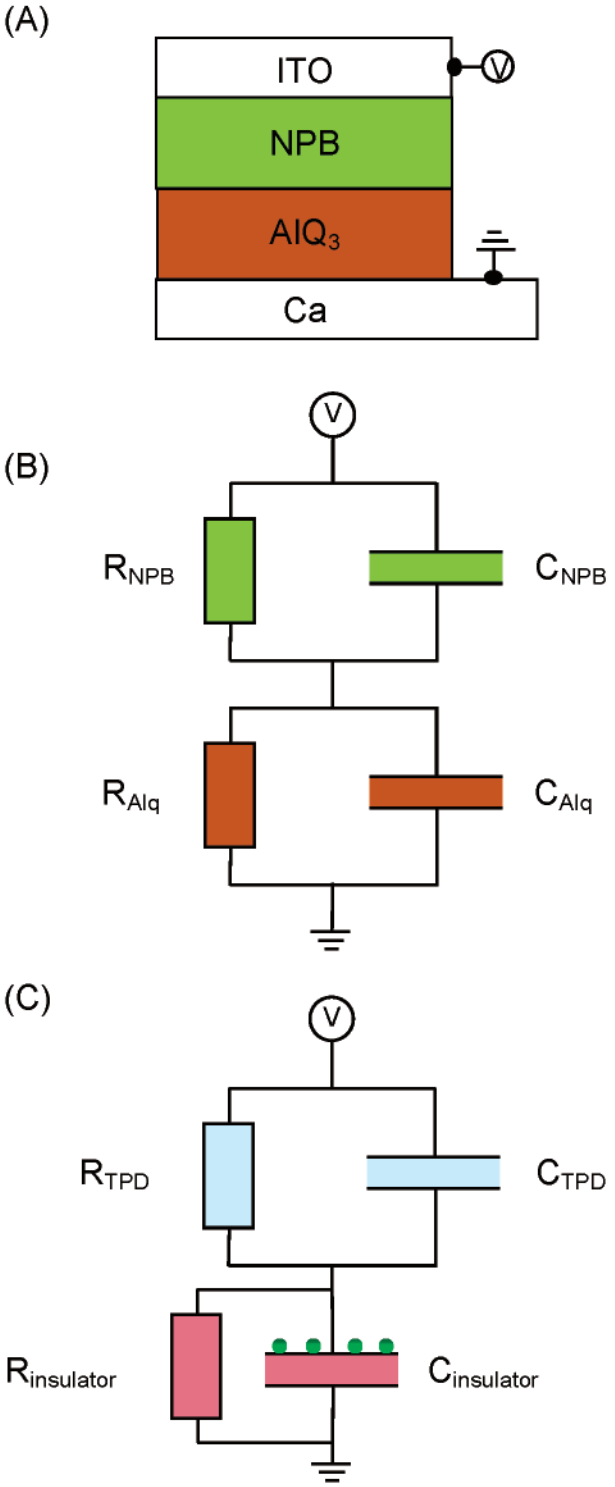

Figure 3. (A) Structure and equivalent circuit for the device studied by Berleb et al., which consists of the following layered structure: ITO/NPB/AlQ_3/Ca. (B) Equivalent circuit for the device shown in (A). The color code corresponds with the colors used in the diagram of the device (see (A)). (C) Equivalent circuit for the device shown in Figure 2. The color code used in the equivalent circuit corresponds to the colors used in the diagram shown in Figure 2.

increase, favoring oxidation of MEH−PPV. Although electrical measurements are not available yet for the device in Figure 2, measurements on an electronically analogous device have been made by Berleb et al.[42,43] For the device in Figure 3A the large work function electrode and hole transport layer combination is comprised of ITO and NPB. These materials are close analogues of, and are electrically similar to, Au and TPD,

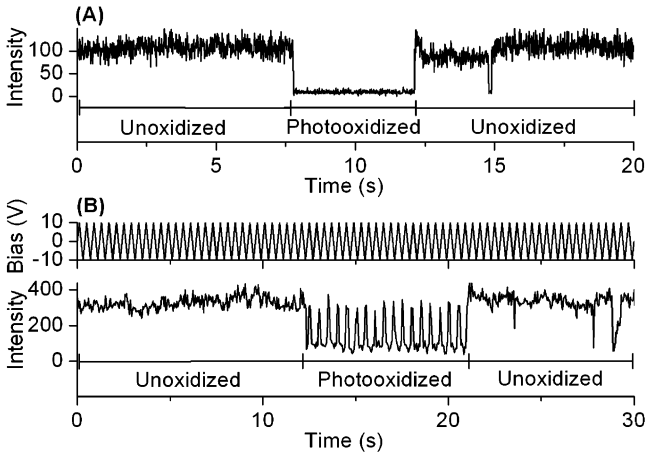

Figure 4. (A) Intensity vs time transient of a single MEH−PPV nanoparticle. No bias is applied. The molecule temporarily resides in a photooxidized state. (B) When a bias is applied on the device, molecules residing in a temporary photooxidized state can recover to their original, unphotooxidized state, fluorescence intensity. The field-induced fluorescence modulation in that period of time is correlated with the repeatedly applied triangle voltage sequence, which is shown in the upper part of panel (B).

respectively. In Figure 3A, the AlQ_3 layer is used for electron transport and electroluminescence and also acts as a hole blocking layer. Extensive capacitance vs voltage ($C-V$) measurements on the device in Figure 3A and closely related devices are reported in the literature.[35,42,43] Berleb et al. have shown that the equivalent circuit shown in Figure 3B is highly consistent with capacitance voltage measurements on multilayer devices of this type.[42,43] The effective resistance R_{NPB} of the hole transporting layer is highly bias-dependent, ranging from 10^8 Ω at negative bias to 360 Ω at positive bias, due to hole doping in NPB. Thus, it seems reasonable to expect that the analogous equivalent circuit in Figure 3C should be qualitatively consistent with our device. At biases comparable to and greater than the inner potential (V_{ip}) holes should be efficiently injected into the device. The amount of charges, Q, and charge density, d, at the interfaces should be given approximately by

$$Q = C(V - V_{ip}) \quad (1)$$

$$\frac{d}{(V - V_{ip})} = \frac{C}{Al} \cong 10^{16} - 10^{17}\text{charges/(V cm}^3\text{)} \quad (2)$$

where C is the geometric capacitance, A is the area of the interface, and l is the depth of the interface, ∼1−10 nm. For the device in Figure 2, charge densities as great as (2−20) × 10^{17} cm^{-3} are predicted for $V = 20$ V which we have routinely achieved.

Basic Observations

Bias-Induced Fluorescence Modulation. MEH−PPV molecules isolated in a PMMA film and irradiated by a continuous wave (CW) laser have been shown to have a time-independent fluorescence intensity on the millisecond to many minutes time scale in the absence of oxygen. However, in the presence of oxygen the fluorescence intensity of MEH−PPV molecules exhibits fluorescence "flickering" due to reversibly formed, long-lived, photooxidized MEH−PPV molecules that contain a photooxidized quenching defect.[11,12] Figure 4A shows an intensity vs time transient for MEH−PPV in a device of the type as shown in Figure 1 and Figure 2 at zero bias. The resulting transients, which are analogous to those of MEH−

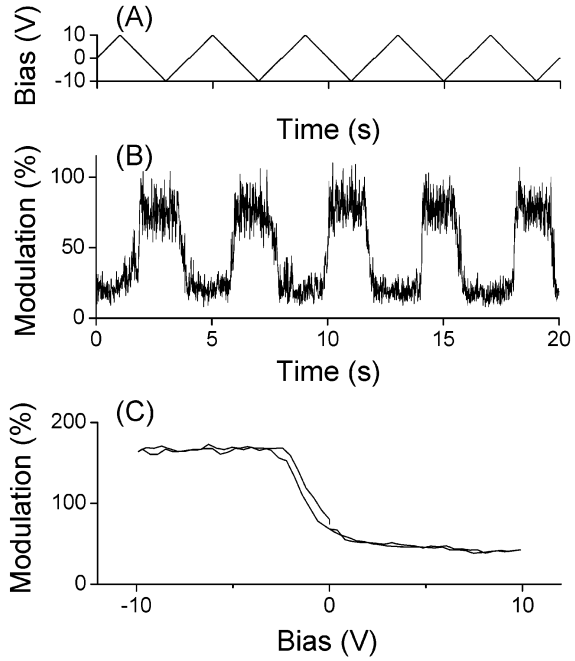

Figure 5. While repeatedly applying a triangle wave voltage sequence (depicted in (A)) on the device, fluorescence transients were collected. These transients, as shown in (B), were averaged over many cycles and replotted as a function of applied bias (C).

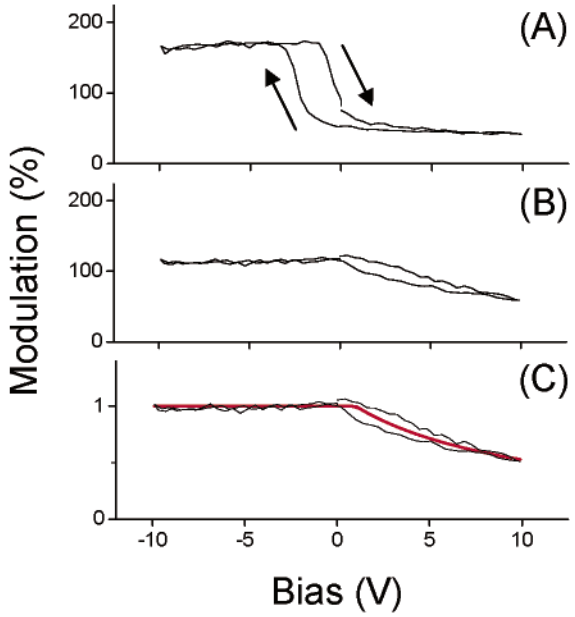

Figure 6. (A),(B) Single molecule field-induced fluorescence modulation plotted versus voltage for photooxidized and pristine unphotooxidized MEH−PPV molecules, respectively. The arrows in (A) indicate the direction of the voltage scan in the plot. (C) Field-induced fluorescence modulation plotted versus voltage for a pristine unphotooxidized MEH−PPV molecule, fitted to eq 4. The best-fit (red) is overlayed on the data.

PPV in an electrodeless PMMA film, exhibit discrete drops in intensity to form long-lived photooxidized (photobleached) states. The flickering behavior was observed to be rare for freshly prepared devices but became more prevalent as the device aged over several days in ambient conditions, presumably due to oxygen diffusion into the device through pinholes in the Au electrode layer. Devices prepared in a vacuum chamber within a glovebox and stored in the glovebox showed considerably less flickering, consistent with the proposed photooxidation origin of this behavior.

The single-molecule fluorescence intensity vs time exhibited a periodic intensity modulation when a periodic triangular time-dependent bias was applied to the device, as shown in Figure 4B. Fluorescence intensity vs time (t) traces were recorded while applying a triangle wave bias voltage sequence (Figure 4 and Figure 5). The bias-induced modulation of the MEH−PPV fluorescence intensity was observed to be highly correlated with the above-mentioned fluorescence flickering/photooxidation process. The electrical bias effect is especially apparent for photooxidized single molecules. Single-molecule traces were averaged over many cycles of the bias, and the data were replotted in the form of an intensity vs bias curve as shown in Figure 5C. For unphotooxidized MEH−PPV molecules, fluorescence quenching was observed at positive bias, see Figure 6B, in analogy to that reported for bulk MEH−PPV devices.[44−46] For neat thin film MEH−PPV, analogous positive bias-induced quenching has been observed and assigned to reversible electron transfer between singlet excitons and holes.[44−46] As described earlier, a "repairing" of photobleaching is observed for negative bias. Negative bias fully repairs the luminescence to its unphotooxidized intensity, see Figure 4B, Figure 5B,C, and Figure 6A. As the single MEH−PPV molecule in Figure 4B became photooxidized at $t = 12$ s, the electric bias-induced modulation of the fluorescence signal significantly increased in magnitude. When the molecule reverted spontaneously to its unoxidized form at $t = 21$ s, the bias-dependent modulation was diminished.

We have previously shown that the discrete sigmoidal behavior in Figure 5C near −1.5 V is indicative of a reversible single-electron transfer event and that the long-lived quencher sites are reversibly oxidized and reduced by the TPD layer at small negative bias. We have also shown that the photobleached form of the polymer is probably a MEH−PPV^+/anion complex formed by photoinduced electron transfer between MEH−PPV and oxygen, forming MEH−PPV^+/O_2^- which is subsequently converted to the chemically more stable MEH-PPV^+/OH^- by interaction with water impurities.

Molecules with No Fluorescence Modulation. About 50% of the single molecules observed in these experiments show very little bias-induced intensity modulation. This is probably due to poor electrical contact between MEH−PPV and TPD. The spin-coating process used herein may bury a significant fraction of MEH−PPV molecules sufficiently deep in the PMMA matrix so that they become electrically insulated from the TPD charge transport layer.

Charges in the Device. Two aspects of the data indicate that the bias-induced intensity effects are due to charges in the device rather than electric field effects, such as field-induced fluorescence quenching due to exciton dissociation.[47] First, the asymmetry of the F−V/SMS data is inconsistent with an electric field effect. Second, the molecules that lack a bias dependence serve as a control, demonstrating the absence of a significant electric field effect. The absence of a field effect is consistent with previous measurements on fluorescence quenching by fields for polymer blends of conjugated polymers in a polymer host, e.g., PMMA. These latter studies have shown that the yield of quenching due to field-induced exciton dissociation approaches zero as the conjugated polymer region approaches single-molecule dimensions.[47] Presumably, the field-induced dissociation process requires conjugated polymer regions large enough to allow for a large electron/hole pair which can be effectively stabilized by the field in order to become energetically accessible. To ensure that the dominant source of intensity variations

during an averaged period of the transient (ignoring photon shot noise) is the bias-induced modulation of the oxidation/reduction state of the molecule, and not "flickering" dynamics, separate synchronous averages were obtained for the unoxidized and photooxidized periods of the intensity vs time traces.

Pristine MEH−PPV Molecules

For unphotooxidized (pristine) molecules (e.g., Figure 6B) the fluorescence intensity was independent of bias for negative bias, but for positive bias showed a gradual decrease in fluorescence intensity with increasing bias. This behavior is highly consistent with the following model for the quenching process:

$$\text{MEH−PPV*} + \text{TPD}^+ \xrightarrow{k_Q} \text{MEH−PPV} + \text{TPD}^+ \quad (3)$$

where the asterisk signifies the presence of a singlet exciton in the nanoparticle, and k_Q is the rate constant for singlet exciton quenching at the TPD/MEH−PPV interface. Holes are well-known quenchers of singlet excitons, involving both charge transfer and energy transfer mechanisms.[45,46,48−50] MEH−PPV nanoparticles are present in the device at the TPD/insulator interface at an extremely low concentration. The HOMO energies of TPD and MEH−PPV are very similar, and certainly within a few kT.[28,41,51] Thus, holes should be much more prevalent in TPD than in MEH−PPV at equilibrium, since the former is present in an enormous excess ($>10^6$). Assuming the validity of eq 3 for the quenching process, the intensity of MEH−PPV should be independent of bias at voltages $<V_{ip}$ when the hole density is relatively small (see eq 1). For biases greater than V_{ip}, however, the $F(V)$ data should be given by

$$\frac{F(V)}{F(V \ll V_{ip})} = \frac{1}{1 + k_Q\tau_0[C(V - V_{ip})/Al]} \quad (4)$$

where τ_0 is the lifetime of a unquenched MEH−PPV molecule (~200 ps).[52,53] This equation in fact reproduces the $F(V)$ data with a best fit k_Q of $(1 \pm 5) \times 10^{-9}$ cm^3 charge^{-1} s^{-1} and $V_{ip} = 0.75 \pm 0.25$ V. The fitting procedure used eq 2 for [TPD$^+$] and an interface depth l of 1 nm. The capacitance of the device $C = 7.6$ nF was calculated from $C = \epsilon_0\epsilon_R A/d$ with $\epsilon_R = 3$, a plate area of 1 cm^2, and a plate separation of 3.5×10^{-7} cm. Assuming diffusion-controlled quenching of MEH−PPV singlet excitons by TPD$^+$, the observed k_Q can be used to determine a quenching radius a from a diffusion-controlled model

$$k_Q = 4\pi Da \quad (5)$$

where D is the diffusion constant, which can be estimated from the Einstein relationship,

$$D = \left(\frac{k_B T}{e}\right)\mu \quad (6)$$

using a typical value for the hole mobility μ in a hole transport layer, i.e., $\mu = 10^{-3}$ cm^2 V^{-1} s^{-1}.[35] The experimentally determined radius ($a = 35-100$ nm) is within an order of magnitude of the actual radius of MEH−PPV (~10 nm). This level of agreement is reasonable considering the many approximations, and supports the assignment of the $F-V$ data at positive bias to a diffusion-controlled quenching process.

Charge-Transfer Kinetics

Basic Formalism. A central result of this paper is that fluorescence intensity vs bias curves of the type shown in Figure 6A,B can be analyzed to study the kinetics of oxidation−reduction processes of single molecules. For simplicity we use the two-state electrode-induced oxidation−reduction of photooxidized MEH−PPV (eq 7) as an example. For the reaction

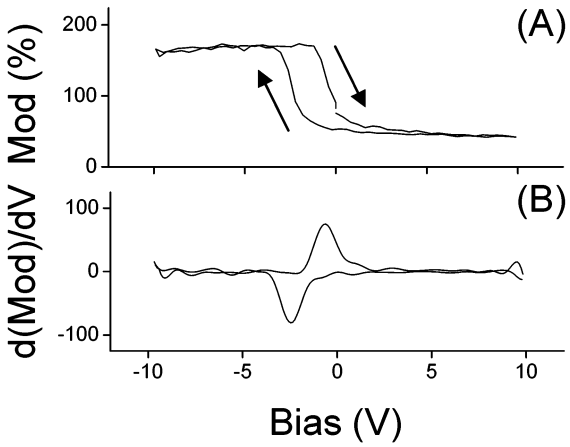

Figure 7. (A) Single molecule field-induced fluorescence modulation plotted versus voltage for a photooxidized MEH−PPV molecule. Taking the derivative of these data as a function of voltage yields the F−V/SMS curve shown in (B), which is reminiscent of a cyclic voltammogram as used in electrochemistry.

$$\text{MEH−PPV/anion} + \text{TPD}^+ \underset{k_{red}}{\overset{k_{ox}}{\rightleftharpoons}} \text{MEH−PPV}^+\text{/anion} + \text{TPD} \quad (7)$$

with k_{ox} and k_{red} the oxidation and reduction rate constants, respectively, the fluorescence intensity $I(t)$ should be a discrete variable having exactly one of two values, I_O and I_R, corresponding to the fluorescence intensity of oxidized and reduced MEH−PPV in the complex at any specific time t depending on whether the molecule is oxidized or reduced, respectively, at that specific time t (when ignoring noise). I_O and I_R are identified with the positive and negative bias-limiting intensity values, e.g., see Figure 5C, respectively. Typically, $I_O \approx 0.3I_R$. Since $I(V)$ is a time-averaged property (over many cycles of the field and the bias vs time of the multichannel scaler), $I(V)$ is a continuous variable, despite the fact that $I(t)$ has discrete values. Consequently,

$$I(V) = PI_O + (1 - P)I_R \quad (8)$$

where P is the time-averaged population of the oxidized form, having any allowed value between 0 and 1. The number of oxidation events per unit time per molecule (R) is given by the relationships

$$P = \frac{I(V) - I_R}{I_O - I_R} \quad (9)$$

and

$$R = \frac{dP}{dt} \quad (10)$$

For the triangular bias scan F−V/SMS technique, R is given by

$$R(V) = S\frac{dP}{dV} \quad (11)$$

where the linear sweep rate $S = dV/dt$ is controlled in the experiment, and dP/dV is the derivative with respect to bias of

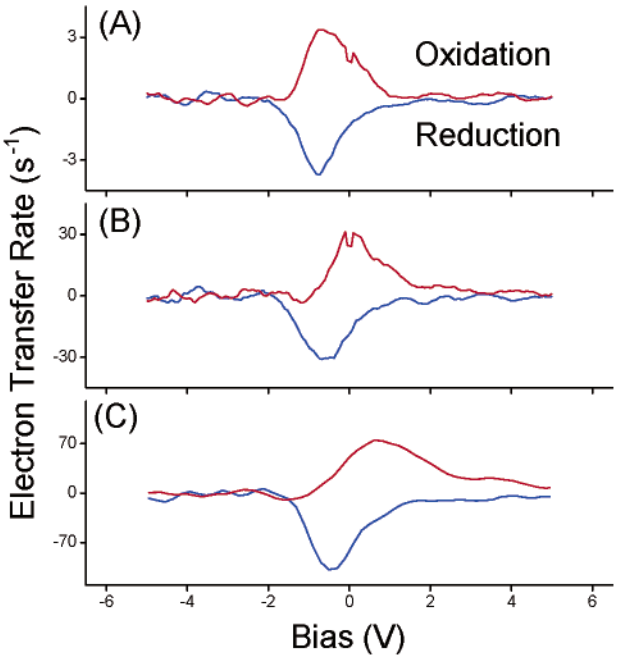

Figure 8. Electron-transfer rate vs voltage curves obtained at different sweep rates for the same molecule. (A) Sweep rate: 5 V/s, (B) sweep rate: 50 V/s, (C) sweep rate: 200 V/s. The oxidation scan (−5 to +5 V) is colored red, the reduction scan (+5 to −5 V) blue. The sweep-rate dependence is apparent upon comparing curves (A−C). The reduction peak potential remains relatively constant with varying sweep rate, while the oxidation peak shifts to higher oxidation potentials with increasing sweep rate. The electron-transfer rates increase with increasing sweep rate. The shift of the oxidation potential to higher bias and the increase of the electron-transfer rate with increasing sweep rate provide evidence that the system is not in equilibrium at these sweep rates.

the *F(V)* data. Figure 7A,B show typical *F(V)* and *R(V)* data, respectively, for a photooxidized MEH−PPV single molecule investigated with a sweep rate $S = 100$ V/s. A sharp peak is observed in the rate data, consistent with a single-electron transfer occurring over a narrow voltage range. The observed hysteresis (comparing forward and reverse scans) indicates that the oxidation/reduction process is not rapid enough to "keep up with" changes of the equilibrium population ($P_{eq}(V)$).

The data in Figure 7B are reminiscent of cyclic voltammetry, which is used to study the kinetics and mechanisms of electrochemical processes. For cyclic voltammetry the rate is manifested by the electrical current *i*. In fact, *R* is closely related to an electrical current, since *R* represents the net number of oxidation events of the single molecule minus the number of reduction events induced by stepping the voltage of the device in the bias sweep. It is important to note that *R* asymptotically approaches zero at high bias, despite the fact that the high bias conditions favor oxidation, see for example the > 4 V region of Figure 8C. The decrease in *R* in this region simply reflects that the "reactant" (MEH−PPV) is fully oxidized by the oxidation−reduction process at the higher voltages. (For electrochemical cells in solution, the current does not approach zero at high bias since diffusion replenishes the reactant molecules at the electrode.)

Photooxidized MEH−PPV. Figure 8 portrays *R* vs bias curves for the same photooxidized molecule using three different sweep rates. The red curves in Figure 8 correspond to the oxidation sweep, i.e., when the bias is linearly swept from −5 V to +5 V, while the blue curves represent the reverse (+5 V to −5 V), reduction sweep. A significant shift between locations of the peaks of the *R* vs *V* curves for the forward vs reverse

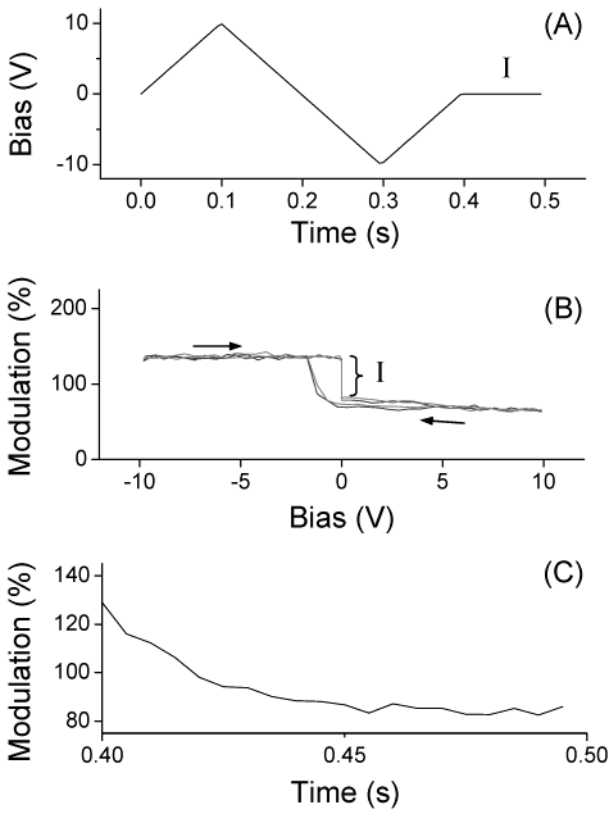

Figure 9. These data were obtained with a zero-bias waiting period at the end of each voltage sweep. The applied voltage sequence is plotted in (A). A 100 ms period at the end the voltage sequence where the sweep rate is 0 V/s is marked by **I**. (B) In the fluorescence modulation vs voltage curve, a steep transition at 0 V bias can be observed, and is indicated by the accolade, with **I** corresponding to the section of the voltage scan indicated by **I** in (A). A slow relaxation of repaired MEH−PPV to the photooxidized state occurred during this 100 ms interval. This is shown in (C), where the fluorescence intensity is plotted as a function of time for the 100 ms resting period in the voltage scan.

sweeps demonstrates that the population *P* of the oxidized state kinetically lags the change in bias of the device. This is especially apparent for the fastest sweep rates (Figure 8C), where the shift (i.e., difference) between the locations of the peaks (V_O and V_R) is 1.1 V. For sufficiently slow sweep rates, the oxidation−reduction process was observed to produce rapidly a nearly equilibrated *R* vs bias curve. Data approaching this situation are shown in Figure 8A. Here the *I(V)* data show a negligible hysteresis when comparing forward and reverse scans; the peaks of the oxidation and reduction "waves" (*R*) are located at the same voltage. The midpoint in the oxidation process for "equilibrated" scans of this type represent the bias ($E_{1/2}$) where the complex spends equal time in the oxidized and reduced forms and the free energy of each form is equal.

The kinetics of the single-molecule oxidation process is particularly apparent in a variant of the time-average intensity vs bias experiment in which the field is held constant for a brief period during each cycle of the sweep (see Figure 9). For this single molecule, the $E_{1/2} \cong -1.5$ V. The zero bias ($V = 0$) equilibrated population is close to unity, i.e., fully oxidized. In the kinetic experiment in Figure 9 the bias was rapidly linearly cycled from 0 to +10 V, down to −10 V, and back to 0 V to produce a nonequilibrium excess population of the reduced form of the molecule ($P \approx 0$) at a time τ_1. The bias was then held at 0 V for a 0.1 s wait period, during which the single-molecule oxidation reaction occurred, as shown in Figure 9C. These data

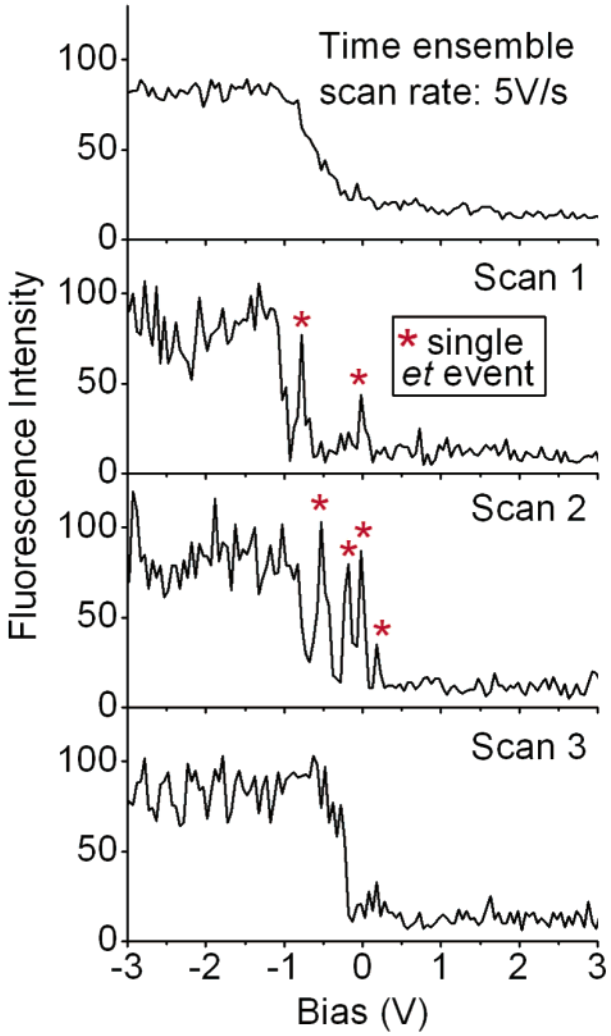

Figure 10. F−V/SMS time-averaged and individual scans of an MEH−PPV single molecule. Red asterisks indicate apparent "partial" single electron-transfer events, and are due to reversible oxidation/reduction within a single dwell time (10 ms).

clearly show that rapid scanning of the bias voltage produces a nonequilibrium ratio of oxidized/reduced forms of the MEH−PPV/anion complex.

The kinetic behavior is complex, however, with oxidation/reduction occurring on several time scales for the same molecule, with kinetic components from the millisecond to hundreds of seconds time scale. Extensive F−V/SMS measurements on a large number of different molecules and devices show that kinetics vary greatly from one molecule to another in the sample, with some molecules showing rapid kinetics while other molecules require a much longer time scale for oxidation/reduction. Other features of the data, such as $E_{1/2}$, $I_{O,}$ and I_R are much less variable. For many molecules the oxidation/reduction rates show a strong increase with bias scan rate in both sweep directions, such that the reactions occur rapidly over a narrow voltage range that is much larger than $E_{1/2}$ for fast scans, as shown in Figure 8.

The relatively slow dynamics of the charge transfer process is apparently analogous to the slow responses observed in $I-V$ curves for OLED devices. For OLEDs slow charging/discharging kinetics have been ascribed to deep hole traps in the charge-transporting layer of the device. Assuming that the same mechanism applies for the single molecule devices described herein, the molecule-to-molecule kinetic variations we have

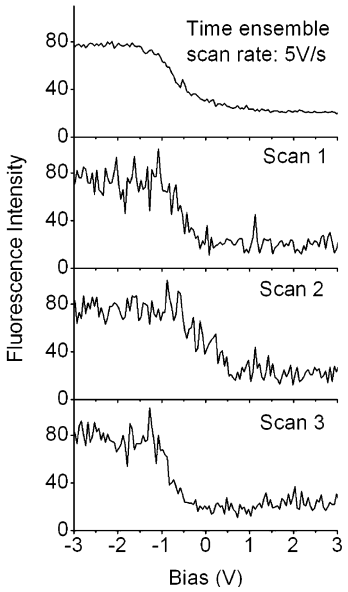

Figure 11. F−V/SMS time-averaged and individual scans of an MEH−PPV single molecule. In this case a smooth transition between the unphotooxidized and photooxidized states exists in both the time-averaged and individual cycles, indicating a fast reversible single electron-transfer process.

observed are due to molecular scale heterogeneity in the hole-trapping effect in the device.

Single-Electron Transfer Events. As shown in Figure 10, F−V/SMS was used to make quantitative rate measurements for single-electron events in single MEH−PPV molecules in the device. The F−V/SMS time-ensemble and single scans for MEH−PPV reveal that the electron transfer process definitely involves a single-electron transfer per molecule. The fluctuations in the transition region between the repaired unphotooxidized state and the photooxidized state, as visible in Figure 10, result from the stochastic nature of electron transfer[54] and not photon shot noise, which is smaller. F−V/SMS data of this type can be used to sort-out the complex mechanism of charge transport, interface charging, and actual electron transfer,[34,35,42,43,55−59] but on a molecule-by-molecule, and location-by-location basis in a device. The spikes marked by a red asterisk indicate the single-electron transfer events. Some of these spikes go all the way up to the unphotooxidized MEH−PPV intensity level, although most spikes reach a lower intensity level. This illustrates that the time scale of the electron transfer for this particular MEH−PPV/anion complex is at the borderline of the 10 ms range, which is the dwell time used to acquire the presented data. In Figure 11 the time ensemble and the single scans all have smooth transitions between the photooxidized and unphotooxidized states during consecutive bias sweeps. In this example, the electron transfer rate is significantly faster than a single dwell time and thus does not show up in the individual scans.

Conclusions

This paper is focused on the further development of the recently introduced SMS/charge injection technique for semiconductor nanoparticle research. F−V/SMS involves simultaneous single molecule fluorescence spectroscopy *and* controllable oxidation/reduction on an individual nanoparticle in an electronic device. The technique which is analogous in several ways to current vs voltage ($I-V$) measurements for devices and electrochemical cells has been applied to the investigation of single molecules (nanoparticles) of the conjugated polymer

MEH−PPV as a function of bias voltage on the device, using a linear sweep rate. Single-electron transfer events were directly observed by F−V/SMS, occurring at the millisecond and faster time scale for MEH−PPV. In addition, F−V/SMS data were recorded as a function of sweep rate to obtain information on both the energetics and kinetics of the charge transfer (oxidation/reduction) process in situ on the nanoscale. The extensive F−V/SMS data presented herein reveal that the dynamics for oxidation/reduction of MEH−PPV nanoparticles are controlled by various factors including filling of deep hole traps in the charge transporting layer of the device, the oxidation/reduction chemical "state" of the MEH−PPV molecule, and the molecular scale heterogeneity of the device.

Acknowledgment. We gratefully acknowledge the National Science Foundation and the Welch Foundation for support of this research.

References and Notes

(1) Kuno, M.; Fromm, D. P.; Hamann, H. F.; Gallagher, A.; Nesbitt, D. J. *J. Chem. Phys.* **2001**, *115*, 1028.
(2) Nirmal, M.; Dabbousi, B. O.; Bawendi, M. G.; Macklin, J. J.; Trautman, J. K.; Harris, T. D.; Brus, L. E. *Nature* **1996**, *383*, 802.
(3) Banin, U.; Bruchez, M.; Alivisatos, A. P.; Ha, T.; Weiss, S.; Chemla, D. S. *J. Chem. Phys.* **1999**, *110*, 1195.
(4) Kuno, M.; Fromm, D. P.; Johnson, S. T.; Gallagher, A.; Nesbitt, D. J. *Phys. Rev. B* **2003**, *67*.
(5) Brokmann, X.; Hermier, J. P.; Messin, G.; Desbiolles, P.; Bouchaud, J. P.; Dahan, M. *Phys. Rev. Lett.* **2003**, *90*.
(6) Moerner, W. E.; Dickson, R. M.; Norris, D. J. *Adv. Atom. Mol. Opt. Phy.* **1998**, *38*, 193.
(7) Lee, T. H.; Gonzalez, J. I.; Dickson, R. M. *Proc. Nat. Acad. Sci. U.S.A.* **2002**, *99*, 10272.
(8) Peyser, L. A.; Vinson, A. E.; Bartko, A. P.; Dickson, R. M. *Science* **2001**, *291*, 103.
(9) Koberling, F.; Mews, A.; Basche, T. *Adv. Mater.* **2001**, *13*, 672.
(10) Hu, D. H.; Yu, J.; Wong, K.; Bagchi, B.; Rossky, P. J.; Barbara, P. F. *Nature* **2000**, *405*, 1030.
(11) Vandenbout, D. A.; Yip, W. T.; Hu, D. H.; Fu, D. K.; Swager, T. M.; Barbara, P. F. *Science* **1997**, *277*, 1074.
(12) Yu, J.; Hu, D. H.; Barbara, P. F. *Science* **2000**, *289*, 1327.
(13) Guillet, T.; Berrehar, J.; Grousson, R.; Kovensky, J.; Lapersonne-Meyer, C.; Schott, M.; Voliotis, V. *Phys. Rev. Lett.* **2001**, *8708*.
(14) Hu, D. H.; Yu, J.; Padmanaban, G.; Ramakrishnan, S.; Barbara, P. F. *Nano Lett.* **2002**, *2*, 1121.
(15) Huser, T.; Yan, M.; Rothberg, L. J. *P. Natl. Acad. Sci. USA* **2000**, *97*, 11187.
(16) Bartko, A. P.; Dickson, R. M. *J. Phys. Chem. B* **1999**, *103*, 3053.
(17) Mehta, A.; Kumar, P.; Dadmun, M. D.; Zheng, J.; Dickson, R. M.; Thundat, T.; Sumpter, B. G.; Barnes, M. D. *Nano Lett.* **2003**, *3*, 603.
(18) Kumar, P.; Mehta, A.; Dadmun, M. D.; Zheng, J.; Peyser, L.; Bartko, A. P.; Dickson, R. M.; Thundat, T.; Sumpter, B. G.; Noid, D. W.; Barnes, M. D. *J. Phys. Chem. B* **2003**, *107*, 6252.
(19) Yan, M.; Rothberg, L. J.; Papadimitrakopoulos, F.; Galvin, M. E.; Miller, T. M. *Phys. Rev. Lett.* **1994**, *73*, 744.
(20) Lowman, G. M.; Daoud, N.; Case, R. M.; Carson, P. J.; Buratto, S. K. *Nano Lett.* **2001**, *1*, 677.
(21) Summers, M. A.; Robinson, M. R.; Bazan, G. C.; Buratto, S. K. *Chem. Phys. Lett.* **2002**, *364*, 542.
(22) Shinohara, K.; Yamaguchi, S.; Wazawa, T. *Polymer* **2001**, *42*, 7915.
(23) Sun, B.; Marx, E.; Greenham, N. C. *Nano Lett.* **2003**, *3*, 961.
(24) Huynh, W. U.; Dittmer, J. J.; Alivisatos, A. P. *Science* **2002**, *295*, 2425.
(25) Mattoussi, H.; Radzilowski, L. H.; Dabbousi, B. O.; Thomas, E. L.; Bawendi, M. G.; Rubner, M. F. *J. Appl. Phys.* **1998**, *83*, 7965.
(26) Dabbousi, B. O.; Bawendi, M. G.; Onitsuka, O.; Rubner, M. F. *Appl. Phys. Lett.* **1995**, *66*, 1316.
(27) Huynh, W. U.; Dittmer, J. J.; Libby, W. C.; Whiting, G. L.; Alivisatos, A. P. *Adv. Functional Mater.* **2003**, *13*, 73.
(28) Campbell, I. H.; Davids, P. S.; Smith, D. L.; Barashkov, N. N.; Ferraris, J. P. *Appl. Phys. Lett.* **1998**, *72*, 1863.
(29) Campbell, I. H.; Smith, D. L.; Neef, C. J.; Ferraris, J. P. *Phys. Rev. B* **2001**, *6403*.
(30) Winder, C.; Lungenschmied, C.; Matt, G.; Sariciftci, N. S.; Nogueira, A. R.; Montanari, I.; Durrant, J. R.; Arndt, C.; Zhokhavets, U.; Gobsch, G. *Synth. Met.* **2003**, *139*, 577.
(31) Nogueira, A. F.; De Paoli, M. A.; Montanari, I.; Monkhouse, R.; Nelson, J.; Durrant, J. R. *J. Phys. Chem. B* **2001**, *105*, 7517.
(32) Guo, X. L.; Choi, J. H.; Tabata, H.; Kawai, T. *Jpn. J. Appl. Phys. Part 2-Lett.* **2001**, *40*, L177.
(33) Park, S.-J.; Gesquiere, A. J.; Yu, J.; Barbara, P. F. *J. Am. Chem. Soc.* **2004**, *126*, 4116.
(34) Nguyen, P. H.; Scheinert, S.; Berleb, S.; Brutting, W.; Paasch, G. *Org. Electronics* **2001**, *2*, 105.
(35) Paasch, G.; Scheinert, S. *Synth. Met.* **2001**, *122*, 145.
(36) Yip, W. T.; Hu, D. H.; Yu, J.; Vandenbout, D. A.; Barbara, P. F. *J. Phys. Chem. A* **1998**, *102*, 7564.
(37) Gross, M.; Muller, D. C.; Nothofer, H. G.; Scherf, U.; Neher, D.; Brauchle, C.; Meerholz, K. *Nature* **2000**, *405*, 661.
(38) Pinner, D. J.; Friend, R. H.; Tessler, N. *J. Appl. Phys.* **1999**, *86*, 5116.
(39) Friend, R. H.; Gymer, R. W.; Holmes, A. B.; Burroughes, J. H.; Marks, R. N.; Taliani, C.; Bradley, D. D. C.; Dos Santos, D. A.; Bredas, J. L.; Logdlund, M.; Salaneck, W. R. *Nature* **1999**, *397*, 121.
(40) Burroughes, J. H.; Bradley, D. D. C.; Brown, A. R.; Marks, R. N.; Mackay, K.; Friend, R. H.; Burn, P. L.; Holmes, A. B. *Nature* **1990**, *347*, 539.
(41) Anderson, J. D.; McDonald, E. M.; Lee, P. A.; Anderson, M. L.; Ritchie, E. L.; Hall, H. K.; Hopkins, T.; Mash, E. A.; Wang, J.; Padias, A.; Thayumanavan, S.; Barlow, S.; Marder, S. R.; Jabbour, G. E.; Shaheen, S.; Kippelen, B.; Peyghambarian, N.; Wightman, R. M.; Armstrong, N. R. *J. Am. Chem. Soc.* **1998**, *120*, 9646.
(42) Berleb, S.; Brutting, W.; Paasch, G. *Org. Electronics* **2000**, *1*, 41.
(43) Berleb, S.; Brutting, W.; Paasch, G. *Synth. Met.* **2001**, *122*, 37.
(44) Yu, J.; Song, N. W.; McNeill, J. D.; Barbara, P. F. *Isr. J. Chem.* **2004**, in press.
(45) McNeill, J. D.; Barbara, P. F. *J. Phys. Chem. B* **2002**, *106*, 4632.
(46) McNeill, J. D.; O'Connor, D. B.; Adams, D. M.; Barbara, P. F.; Kammer, S. B. *J. Phys. Chem. B* **2001**, *105*, 76.
(47) Deussen, M.; Scheidler, M.; Bassler, H. *Synth. Met.* **1995**, *73*, 123.
(48) Yu, J.; Song, N. W.; McNeill, J. D.; Barbara, P. F. *Isr. J. Chem.*, in press.
(49) Lammi, R. K.; Ambroise, A.; Wagner, R. W.; Diers, J. R.; Bocian, D. F.; Holten, D.; Lindsey, J. S. *Chem. Phys. Lett.* **2001**, *341*, 35.
(50) Tessler, N. *Adv. Mater.* **1999**, *11*, 363.
(51) Campbell, I. H.; Hagler, T. W.; Smith, D. L.; Ferraris, J. P. *Phys. Rev. Lett.* **1996**, *76*, 1900.
(52) Zhang, H. R.; Lu, X. F.; Li, Y.; Ai, X. C.; Zhang, X. K.; Yang, G. Q. *J. Photochem. Photobiol., A−Chemistry* **2002**, *147*, 15.
(53) Yang, G.; Li, Y.; White, J. O.; Drickamer, H. G. *J. Phys. Chem. B* **1999**, *103*, 5181.
(54) Barbara, P. F.; Meyer, T. J.; Ratner, M. A. *J. Phys. Chem.* **1996**, *100*, 13148.
(55) Nesterov, A.; Paasch, G.; Scheinert, S.; Lindner, T. *Synth. Met.* **2002**, *130*, 165.
(56) Paasch, G.; Peisert, H.; Knupfer, M.; Fink, J.; Scheinert, S. *J. Appl. Phys.* **2003**, *93*, 6084.
(57) Paasch, G.; Scheinert, S. *Synth. Met.* **2003**, *135*, 407.
(58) Paasch, G.; Nesterov, A.; Scheinert, S. *Synth. Met.* **2003**, *139*, 425.
(59) Scheinert, S.; Paasch, G.; Doll, T. *Synth. Met.* **2003**, *139*, 233.